Photoisomerization of Azobenzene Derivatives in Nanostructured Silica

Paul Sierocki,[†] Huub Maas,[‡] Patrick Dragut,[§] Gabriele Richardt,[§] Fritz Vögtle,*[,§] Luisa De Cola,*[,‡,||] Fred (A. M.) Brouwer,[‡] and Jeffrey I. Zink*[,†]

Department of Chemistry and Biochemistry, University of California Los Angeles, 607 Charles E. Young Drive East, Los Angeles, California 90095-1569, Van 't Hoff Institute for Molecular Sciences, University of Amsterdam, Nieuwe Achtergracht 166, 1018 WV Amsterdam, The Netherlands, and Kekulé-Institut für Organische Chemie und Biochemie der Universtät Bonn, Gerhard-Domagk-Strasse 1, D-53121 Bonn, Germany

Received: July 1, 2006; In Final Form: September 7, 2006

A series of derivatized azobenzene molecules are synthesized such that one of the phenyl groups can be chemically bonded to mesostructured silica and the other, derivatized with dendrons, is free to undergo large-amplitude light-driven motion. The silica frameworks on which the motion takes place are either 150 nm thick films containing ordered hexagonal arrays of tubes (inner diameter about 2 nm) containing the bonded azobenzenes, or particles (about 500 nm in diameter) containing the same ordered arrays of functionalized tubes. The photoisomerization yields and the rate constants for the thermal cis to trans back-reaction of the azobenzenes in the tubes are measured and compared to those of the molecules in solution. The rate constants decrease with increasing size of the dendrons. Fluorescence spectra of the cis and trans isomers in the pores show that the photoisomerization in the nanostructured materials is selectively driven by specific wavelengths of light and is reversible.

Introduction

Functional systems that show a controlled response to light have a large potential in technical applications because of the noncontact manipulation of the material. Light-induced processes can induce small changes at the molecular scale that cause a modification in the macroscopic properties. This photoresponsive material could be of importance in fields such as optical switches,[1,2] nanovalves,[3−4] site-related drug release,[5] chemical sensing,[6] optical data storage,[7−8] and light-powered molecular machines.[9,10] Combining inorganic and organic systems to create hybrid composites leads to innovative materials with unique properties.[11−22]

Azobenzene has attracted considerable interest over the past few decades. The light-driven trans/cis isomerization has been used to determine the local free volume in polymer systems,[23] to construct holographic materials,[24] and to prepare photoresponsive surfactants.[25] Recently, azobenzene has been tethered to the wall of an ordered nanoporous membrane.[4] The azobenzene-functionalized nanocomposite material has an optically switchable pore size that has been shown to photoregulate mass transport through this membrane.[3]

If a large organic dendron is attached to one end of the azobenzene molecule and the other end is anchored to a support, photoisomerization will cause movement of the dendron. The well-known reversible light-driven isomerization of the azobenzene derivatives is used as a tool to create a light-responsive functional material. In the azo-functionalized nanostructured silica a supramolecular arrangement is achieved where the light-induced change of individual molecules causes a change of the entire material property. This motion can also be utilized to impel molecules through a nanopore or to trap and release molecules.

To get a good insight of the mechanism and functionality of the material, a series of strategically functionalized compounds was synthesized and examined. The studied molecules are shown in Scheme 1. The rate constant for the thermal cis to trans isomerization is measured, the isomerization yields are calculated, and the low temperature fluorescence emission in frozen glass matrices is studied. The molecules are then covalently attached to the pore wall of MCM-41 and two-dimensional (2D) hexagonal thin films. The thermal cis to trans isomerization is measured and the fluorescence again studied. Comparisons of rate constants and emission for the azobenzene derivatives in solution and in the ordered nanopores are made.

The azobenzene derivatives range in size from **AzoOH** (MW = 228 g/mol, diameter = 1.2 nm, volume = 147 Å^3) to **AzoG3** (MW = 1820 g/mol, diameter = 3.4 nm, volume = 1407 Å^3).[26] All molecules have a benzylic alcohol functionality which is used to anchor them to the silica through the formation of a carbamide derivative to the linker molecule (ICPES).

Experimental Section

I. Synthesis of Azobenzene Derivatives. 3,5-Bis(benzyloxy)-benzyl alcohol (**G1**),[27,28] 3,5-bis[3′,5′-bis(benzoyloxy)benzoyloxy]benzyl alcohol (**G2**),[27,28] 4-(4′-hydroxyphenolazo)benzyl alcohol (**AzoOH**),[29] 4-(4′-methoxyphenylazo)benzyl alcohol (**AzoOMe**),[30] and 4-(4′-(3″,5″-bis(3‴,5‴-bis(benzolyoxy)benzoyloxy)benzoyloxy)phenylazo)benzyl alcohol (**AzoG2**)[30] have been prepared according to the literature indicated.

*General Procedure for the Preparation of **AzoG0**, **AzoG1**, and **AzoG3**.* To a solution of 4-(4′-hydroxyphenylazo)benzyl alcohol, appropriate substituted benzylic bromide, [18]crown-6,

* Corresponding authors. Telephone: +31 205256439. E-mail: ldc@science.uva.nl (l.d.c.); voegtle@uni-bonn.de (f.v.); zink@chem.ucla.edu (j.i.z.).

† University of California Los Angeles.

‡ University of Amsterdam.

§ Kekulé-Institut für Organische Chemie und Biochemie der Universtät Bonn.

|| Present address: Westfälische Wilhelms-Universität Münster, Physikalishes Institut, Mendelstrasse 7, D-48149 Münster, Germany.

10.1021/jp0641334 CCC: $33.50
Published on Web 11/11/2006

SCHEME 1: Chemical Structures of the Studied Azo Compounds and Reference Dendrons

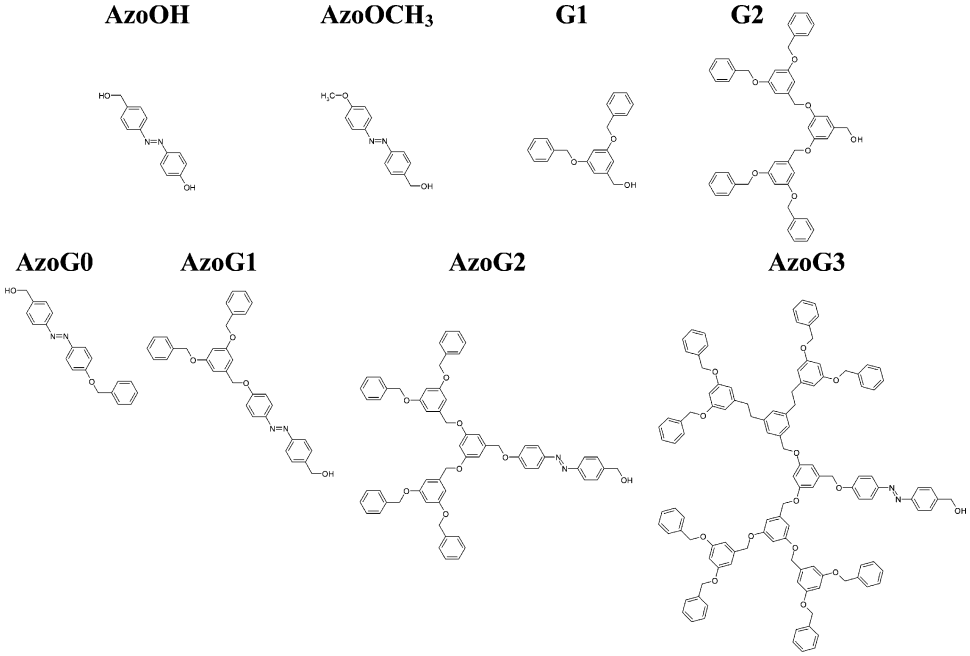

and acetone followed by K_2CO_3 were added in the amounts indicated below. The reaction mixture was refluxed for 24 h under argon atmosphere. After removal of the solvent under reduced pressure, the resulting solid residue was portioned between water and chloroform. The organic layer was separated; the aqueous layer was further extracted with chloroform and washed three times with brine and water. The combined organic layers were finally dried with sodium sulfate. After removal of the solvent, the crude compound was purified on a silica gel column.

*4-(4′-(Benzyloxy(phenylazo)benzyl Alcohol (**AzoG0**).* To 4-(4′-hydroxyphenylazo)benzyl alcohol (200 mg, 0.877 mmol), benzyl bromide (104 mL, 0.877 mmol), [18]crown-6 (46 mg, 0.18 mmol), acetone (44 mL), and K_2CO_3 (181 mg, 1.31 mmol) were added.

The crude product was purified by repeated flash chromatography (dichloromethane, 3% diethyl ether) to give 209 mg (75%) of a reddish-yellow powder (mp 164−165 °C). ^{1}H NMR (300 MHz, $CDCl_3$, 25 °C): δ [ppm] = 4.7 (s, 2H, CH_2OH), 5.0 (s, 2H, OCH_2−C_6H_5), 7.0 (d, 2H), 7.25−7.45 (m, 7H), 7.7−7.9 (m, 4H). ^{13}C NMR (100.6 MHz, $CDCl_3$, 25 °C): δ [ppm] = 64.9 (CH_2OH), 70.3 (OCH_2−C_6H_5), 115.1, 122.8, 124.7, 127.4, 127.5, 128.1, 128.6, 137.1, 143.0, 147.2, 152.2, 161.1 (C_{ar}). IR (KBr pellet, cm^{-1}): ν N═N 1580.9. MS (GC/MS (EI)): m/z = 318 ($M^+ + H$). Anal. Calcd for $C_{20}H_{18}N_2O_2$ (318.37): N, 8.79; C, 75.45; H, 5.7. Found: N, 8.753; C, 75.16; H, 5.85.

*4-(4′-(3″,5″-Bis(3‴,5‴-Bis(benzyloxy)benzyloxy)phenylazo)-benzyl Alcohol (**AzoG1**).* To 4-(4′-Hydroxyphenylazo)benzyl alcohol (269 mg, 1.17 mmol), F-**G1**-Br[27,28] (450 mg, 1.17 mmol), [18]crown-6 (62 mg, 0.23 mmol), acetone (55 mL), and K_2CO_3 (244 mg, 1.76 mmol) were added.

The crude product was purified by flash chromatography (dichloromethane, 3% diethyl ether) to give 458 mg (74%) of an orange powder (mp 121−123 °C). ^{1}H NMR (300 MHz, $CDCl_3$, 25 °C): δ [ppm] = 4.6 (s, 2H, CH_2OH), 4.9 (s, 6H, OCH_2−C_6H_5−), 6.45 (s, 1H, H_{ar}), 6.55 (s, 2H, H_{ar}), 6.9 (d, 2H, H_{ar}), 7.19−7.35 (m, 12H, H_{ar}), 7.7−7.85 (m, 4H, H_{ar}). ^{13}C NMR (100.6 MHz, $CDCl_3$, 25 °C): δ [ppm] = 64.8 (CH_2OH), 70.2 (OCH_2−C_6H_5), 101.7, 106.4, 115.2, 122.8, 124.8, 127.4, 127.5, 128.0, 128.6, 136.8, 138.9, 143.3, 147.2, 152.2, 160.2, 161.1 (C_{ar}). IR (KBr pellet, cm^{-1}): ν N═N 1597. GC/MS (quadrupole/EI): m/z = 530 (M^+). Anal. Calcd for $C_{34}H_{30}N_2O$ (530.61): C, 76.96; H, 5.698; N, 5.279. Found: C, 77.06; H, 5.812; N, 5.168.

*4-(4′-(3″,5″-Bis(3‴,5‴-bis(3⁗,5⁗-bis(benzyloxy)benzyloxy)-benzyloxy)benzyloxy)phenylazo)benzyl Alcohol (**AzoG3**).* To 4-(4′-hydroxyphenylazo)benzyl alcohol (57 mg, 0.247 mmol), F-**G3**-Br[27,28] (200 mg, 0.247 mmol), [18]crown-6 (13 mg, 0.05 mmol), acetone (14 mL), and K_2CO_3 (51 mg, 0.37 mmol) were added.

The crude product was purified by flash chromatography (dichloromethane, 3% diethyl ether) to give 267 mg (60%) of an orange solid (mp 128−129 °C). ^{1}H NMR (400 MHz, $CDCl_3$, 25 °C): δ [ppm] = 4.45 (s, 2H), 4.8 (s, 10H), 4.9 (s, 20H), 6.45 (m, 7H), 6.55 (m, 14H), 6.9 (m, 4H), 7.1−7.3 (m, 34H), 7.39 (m, 4H), 7.71−7.82 (m, 7H). IR (KBr pellet, cm^{-1}): N═N, 1595. MS (FAB) *m*-NBA; m/z = 1804.6 (M^+). Anal. Calcd for $C_{118}H_{102}N_2O_{18}$ (1804.08): C, 78.56; H, 5.70; N, 1.55. Found: C, 78.11; H, 5.885; N, 1.574.

II. Nanostructured Materials. *A. Prehydrolyzed Sol and 2D Hexagonal Thin Film Preparation.* The tetraethylorthosilicate (TEOS) and cetyltrimethylammonium bromide (CTAB) were purchased from Aldrich and used without further purification. Isocyanopropyltriethoxysilane (ICPES) was purchased from Aldrich and purified by distillation before use. Absolute EtOH was purchased from Pharmco Products Inc. and is ACS grade. The toluene and dichloromethane used for the frozen glass experiments were purchased from Merck and are ACS grade. The silicon wafers used as substrates were purchased from Silicon Quest International. They were soaked in a 4:1 solution of sulfuric acid and 30% hydrogen peroxide for 1 h, rinsed with deionized water, and dried with nitrogen.

The initial sols were prepared in two steps. First, a prehydrolyzed TEOS sol was prepared by heating at 60 °C for 1 h TEOS, EtOH, HCl, and H_2O in the molar ratio 1:3:5 × 10^{-5}:1. To a portion of the prehydrolyzed sol was added CTAB, EtOH, HCl, and H_2O so that the final molar composition was 1 TEOS:20 EtOH:0.004 HCl:5 H_2O:0.10 CTAB. The sol was stirred at room temperature for 15 min and aged for 1 day. The

azodendrimer was reacted with ICPES by refluxing in dry toluene for 3 h. This solution was added directly to the sol, giving an azodendrimer concentration of ~1.5 mM. The triethoxysilane moiety co-condenses with the silica framework so that the machine is attached to the pore wall with the azodendrimer extending into the hydrophobic interior of the micelle. The films were deposited by dip coating onto ⟨100⟩ silicon with a resistivity >15 ohm·cm at a rate of 5 cm/min in a humidity-controlled chamber (relative humidity (RH) 50%). The films were dried at room temperature and 50% RH for 2 days. A Soxhlet extraction using EtOH was then performed to remove the surfactant from the films, leaving them mesoporous. In an alternative procedure the films were prepared as described above but were then calcined at 400 °C for 4 h to remove the surfactant. The ICPES was attached to the films using a vapor deposition procedure.[15,31] The films were then soaked in toluene to remove any unattached ICPES, and the azo derivative was attached by refluxing the films in a 1 mM solution of the azodendrimer in toluene for 4 h. The films were again soaked in fresh toluene to remove any unattached azodendrimer and dried at room temperature for 1 day.

B. 2D Hexagonal Silica Powder Preparation. The synthesis was performed in accordance with published procedures.[32] In a typical procedure, 2.5 g of CTAB was dissolved in 50 mL of deionized water by heating gently. The solution was then cooled to room temperature, and 13.2 g of ammonia hydroxide and 60 g of ethanol were added and stirred for 15 min. Then 4.67 g of TEOS was added quickly while stirring, and the mixture was stirred for an additional 2 h. The slurry was suction filtered, rinsed with two 100 mL portions of deionized water followed by two 100 mL portions of methanol, and dried overnight at 90 °C. The powder was then calcined at 550 °C for 5 h to remove the CTAB. ICPES was attached using a modified version of the vapor deposition procedure described in the Experimental Section for the thin films[31] followed by soaking in toluene to remove any unattached ICPES. The azodendrimer was then attached by refluxing the powder in a 1 mM solution of the azodendrimer in toluene for 12 h, rinsed in toluene to remove any unattached azodendrimer, and dried at room temperature under vacuum.

III. Sample Characterization and Analysis. *A. Low Temperature Emission Spectroscopy.* Samples were cooled using a Displex closed-cycle helium refrigerator. The emitted light was passed through a single monochromator (Spex). A cooled RCA C31034 photomultiplier tube was used to detect the signal, which was then fed into a Stanford Research Systems SR400 photon counter and stored in a computer. The samples were excited with the 351 nm line from a krypton ion laser, the 457 nm line from an argon ion laser, or the 257 nm line from a frequency-doubled argon ion laser. The frozen glass samples were prepared as follows: the azodendrimer was added to a 1:1 solution of toluene and dichloromethane to give a solution of known concentration. The solution was then added to a capillary tube and frozen with liquid nitrogen. The capillary tube was then flame sealed and tested for leaks under vacuum.

B. Ultraviolet/Visible Spectroscopy. Room temperature UV−Vis spectra were recorded on a Cary 400 spectrophotometer.

C. Photochemistry. Samples were irradiated with a monochromated Hg light source from a Spex fluorolog. Quantum yields for photoisomerization were determined by actinometry with Aberchrome 540 under 344 nm (forward reaction) and 450 nm (reverse reaction) irradiation.

D. Grazing Incidence Angle X-ray Diffraction (GIAXRD). GIAXRD measurements were performed on a Panalytical X'Pert Pro powder diffractometer. The radiation source is copper ($K\alpha_1$ and $K\alpha_2 = 1.5418$ Å).

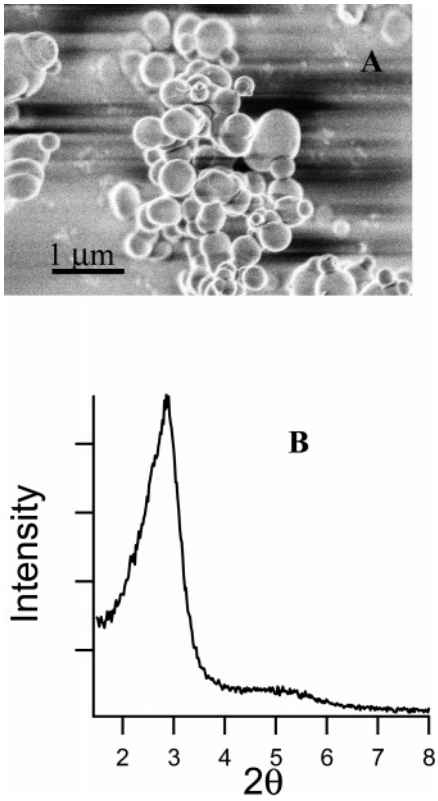

Figure 1. (A) SEM image of MCM-41 submicron spheres. (B) XRD pattern of calcined MCM-41.

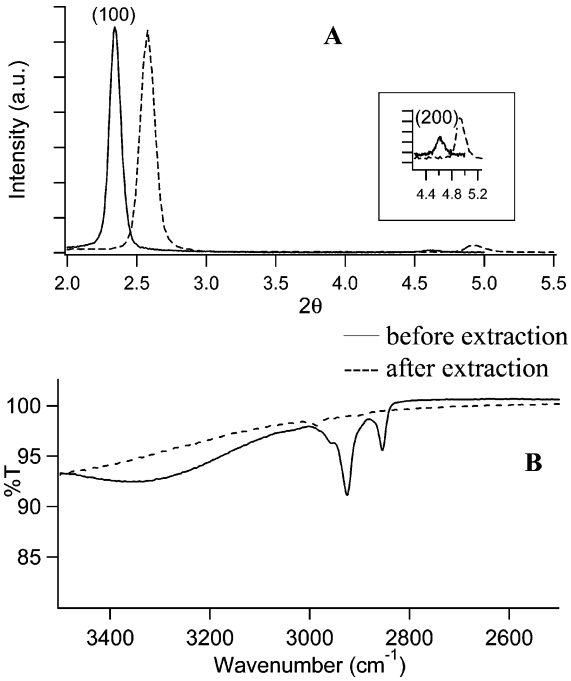

Figure 2. (A) XRD pattern of film before and after solvent extraction. (B) FTIR spectrum of film before and after solvent extraction.

E. Characterization of Azobenzene Derivatives. Melting temperatures were determined using a Büchi SMP-20. IR spectra were recorded on a Perkin-Elmer FT-IR Paragon 500 spectrometer. NMR spectra were recorded on a Bruker Avance 300 (^{1}H NMR, 300 MHz) and Bruker AM 400 (^{1}H NMR, 400 MHz; ^{13}C NMR, 100.6 MHz), EI mass spectra were measured on a MS-30 and MS-50, A.E.I. Manchester, Great Britain. FAB mass

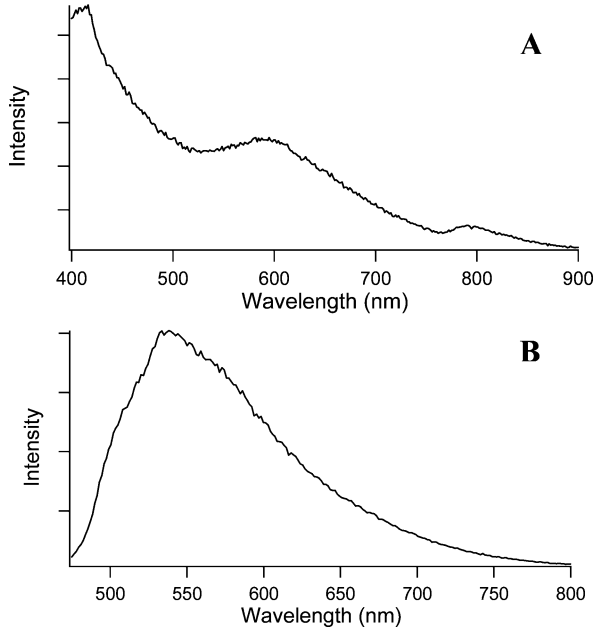

Figure 3. Luminescence spectra of **AzoG1**-derivatized MCM-41 excited at 351 (A) and 457 nm (B).

spectra were recorded on a Concept 1H, Kratos Analytical Ltd., Manchester, Great Britain. GC-MS spectra were recorded on a gas chromatograph HP 5850, Serie II, and a mass spectrometer HP 5989 A, Hewlett-Packard, Palo Alto, CA. Elemental analyses were obtained at Bonn University, Kekulé-Institute, on an elementar vario EL.

Results

I. Materials. Properties were studied in two types of nanostructured silicates: MCM-41 (ordered mesoporous silica spheres) and 2D hexagonal thin films.

A. MCM-41. A scanning electron micrograph (SEM) image of the submicron SiO_2 spheres is shown in Figure 1A. The X-ray diffraction pattern of the powder is shown in Figure 1B. The first-order diffraction peak appears at $2\theta = 2.86°$ with a corresponding lattice spacing of 31 Å. The observed diffraction peak is consistent with those reported in the literature for submicron SiO_2 spheres with an ordered hexagonal pore system.[33]

B. 2D Hexagonal Thin Films. The X-ray diffraction pattern for the 2D hexagonal thin films is shown in Figure 2A. For the as-prepared material a diffraction peak is observed at $2\theta = 2.3°$ corresponding to a lattice spacing of 38 Å. The solvent extracted material shows a slight shift in *d*-spacing to 34 Å. The Fourier transform infrared (FTIR) spectrum is used to monitor the extent of template removal in the thin films by monitoring the disappearance of the CH_2 stretches of the aliphatic tail of CTAB at 2850 and 2925 cm^{-1} (Figure 2B).

II. Spectroscopy. *A. MCM-41.* The low temperature (40 K) emission spectra of **AzoG1** tethered to the pore wall of MCM-41 are shown in Figure 3. The spectrum of **AzoG1**-derivatized MCM-41 excited at 351 nm contains a peak centered at 425 nm and a less intense broad peak at 600 nm (Figure 3A). The emission spectrum obtained with 457 nm excitation is shown in Figure 3B. A broad featureless peak with a maximum at 535 nm is observed.

B. 2D Hexagonal Thin Films. The low temperature emission spectra (Figure 4) of the **AzoG1**-derivatized thin films exhibit the same characteristic peaks as those of the **AzoG1**-derivatized MCM-41. The process is reversible, and 457 or 257 nm excitation can be used to generate the trans isomer.

C. Frozen Glass Emission Spectra of Azo Derivatives. The emission spectra of the azo derivatives in the frozen glass are used to assist in assigning the emission spectra obtained from the azo derivatives in the pores of the MCM-41 or thin films. Figure 5 shows the emission of **AzoG3** in a 1:1 toluene: dichloromethane frozen glass with 351 (A) and 457 nm (B) excitation.

The emission spectrum of the least concentrated glass excited at 351 nm contains a vibronically structured emission band between 400 and 500 nm. A concentration-dependent peak grows in as the **AzoG3** concentration is doubled. When the concentration is increased by an order of magnitude, a peak centered at 760 nm is observed. With excitation at 457 nm, a peak with vibronic structure is observed at 550 nm. As the concentration is doubled, some of the vibronic structure is lost and the peak red shifts. Increasing the **AzoG3** concentration by an order of magnitude results in a spectrum characterized by a broad featureless peak centered at 710 nm.

The low temperature emission spectra of the dendron (**G1**) which lacks the azo moiety is shown in Figure 6. A vibronically

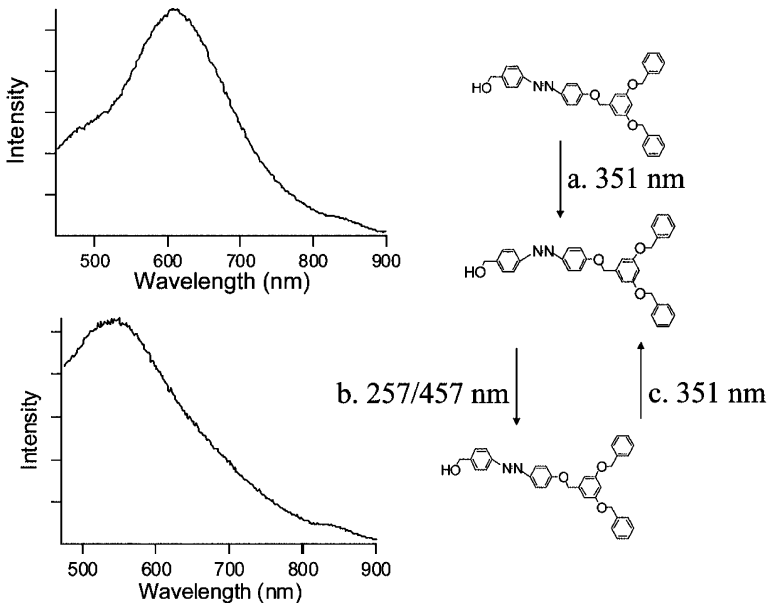

Figure 4. Emission spectra of **AzoG1** upon irradiation at 351 and 457/257 nm in a 2D hexagonal thin film.

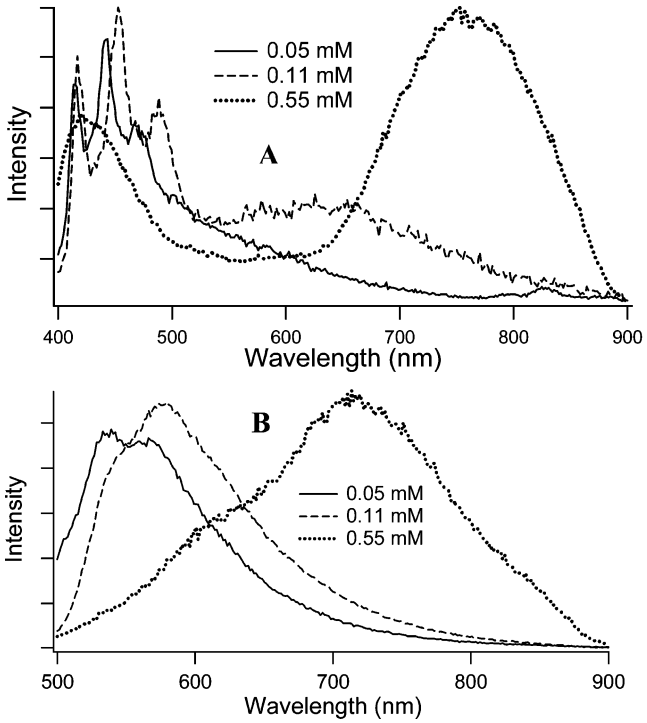

Figure 5. Concentration dependence of **AzoG3** emission in 1:1 CH_2Cl_2:toluene frozen glass (40 K). (A) Excitation at 351 nm; (B) excitation at 457 nm.

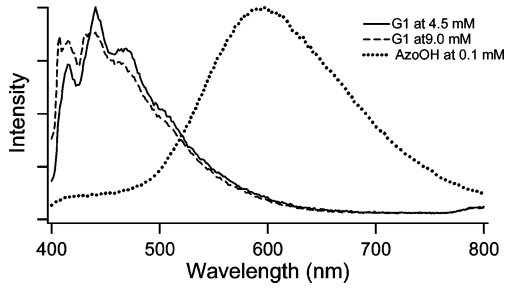

Figure 6. Low temperature emission from Fréchet dendron **G1** in frozen glass (1:1 CH_2Cl_2:toluene) with excitation at 351 nm compared to **AzoOH** emission.

structured emission band is observed at 450 nm, but no concentration-dependent peak is found at 600 nm. **AzoOH** lacks the dendron, so comparisons can be made with **G1** (which lacks the azo group). The **AzoOH** spectrum is dominated by a broad featureless peak centered at 600 nm.

III. Isomerization Quantum Yields. The quantum yield for isomerization is given by[34,35]

$$\varphi = k_0 \frac{1}{I_0} \frac{1}{1 - 10^{-\epsilon c l}} \qquad (1)$$

where k_0 is a zero-order rate constant for the decrease of the initial isomer concentration in mol L^{-1} s^{-1}, I_0 is the intensity of incident irradiation light in einstein L^{-1} s^{-1}, ϵ is the extinction coeffiecient in L mol^{-1} cm^{-1} at the irradiation wavelength of the solution, c is the concentration of this solution in mol L^{-1}, and l the path length of the light through the sample in cm. The concentration of the cis and trans isomers were determined from the absorbance values at different irradiation times as shown in the Supporting Information. The sample was first brought into a photostationary equilibrium with 344 nm light. The sample was then irradiated at 450 nm for a period of time. The absorption spectra were taken at 60 s intervals up to 900 s.

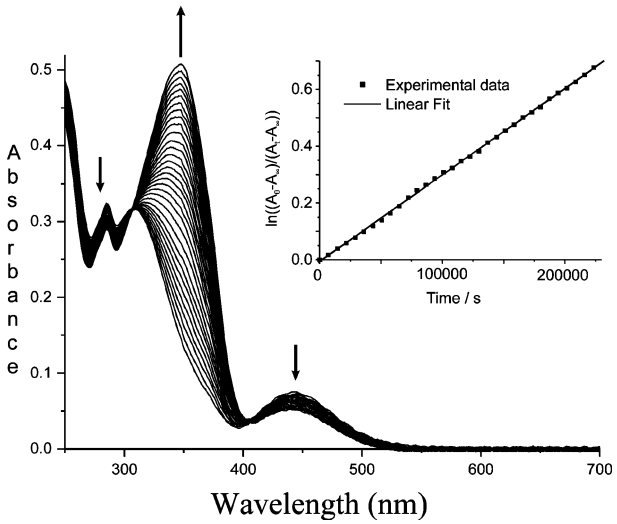

Figure 7. Absorbance evolution of **AzoG1** as a function of time after irradiation with 344 nm light to reach the photostationary state. The inset shows a linear fit of eq 2 using the absorption data at 350 nm.

The calculation of the isomerization quantum yield is discussed in section III.B under Discussion.

IV. Rate Constant for Thermal cis → trans Isomerization. The change in absorption over time for **AzoG1**, in CH_2Cl_2 solution, that had been photoisomerized with ultraviolet radiation into a photostationary state is shown in Figure 7. The $\pi\pi^*$ absorption band of the trans isomer (350 nm) gains intensity, while the $n\pi^*$band of the cis isomer (450 nm) loses intensity.

Discussion

I. Materials. *Nanostructured Framework.* The properties of the azobenzene derivatives in the nanostructured material were studied in MCM-41 and templated 2D hexagonal silica thin films. MCM-41, discovered in 1992, consists of submicron-size silica spheres.[36] It exhibits a regular pore system which consists of an array of unidimensional, hexagonally shaped pores with a narrow pore size distribution. The lattice spacing is approximately 3 nm when CTAB is used as the templating agent. The pore walls are composed of amorphous silica.[36]

The films used in this paper are prepared by dip coating. The sols are diluted and the concentration of reagents is designed to prevent fast condensation of the inorganic precursor. During deposition by dip coating, a layer of solution is dragged onto the substrate surface. The alcohol and then the water evaporate from the film/air interface, causing the concentration of inorganic precursor, acid, and surfactant to increase gradually. The mesostructure of the film forms via evaporation-induced self-assembly.[37−39] The solvent evaporation induces the formation of micelles and their self-assembly with the inorganic species. Polycondensation forms the solid silica framework that holds the network together. The azo derivative attaches itself to the surface of the pore using ICPES as the linker molecule with the dendrimer extending into the hydrophobic interior of the micelle. The X-ray diffraction (XRD) pattern of the as-prepared material shows a strong diffraction peak at $2\theta = 2.3°$ (corresponding to a d-spacing of 38 Å), which can be indexed to the (100) reflection of the hexagonal mesostructure. A weak (200) reflection at $2\theta = 4.6°$ is evidence of long-range order in the films. The absence of (110) and (210) reflections suggests that the films have an oriented hexagonal mesostructure with cylindrical pores aligned parallel to the substrate surface. A subsequent Soxhlet extraction affords the mesoporous material with the azobenzene derivative still attached. XRD results

TABLE 1: Photophysical Properties of Azobenzene Derivatives in CH_2Cl_2 Solutions at Room Temperature

compound	λ_{max} [nm]	$\epsilon(\lambda_{max})$ [M^{-1} cm^{-1}]	$\varphi_{t\to c}^{344}$	$\varphi_{c\to t}^{344}$	$\varphi_{t\to c}^{450}$	$\varphi_{c\to t}^{450}$	k_Δ [s^{-1}]
AzoOH	346	25 800	0.20				5.84×10^{-4}
$AzoOCH_3$	350	29 600	0.18	0.04	0.81	0.57	5.19×10^{-6}
AzoG0	351	26 600	0.33	0.03	0.40	0.61	3.32×10^{-6}
AzoG1	351	28 700	0.31	0.05	0.36	0.64	3.05×10^{-6}
AzoG2	350	28 900	0.25	0.15	0.23	0.49	3.06×10^{-6}
AzoG3	349	41 700	0.13	0.02	0.02	0.30	2.60×10^{-6}

(Figure 2A) show existence of the ordered mesostructure (with a slight shift in *d*-spacing to 34 Å), while the FTIR spectra of the material before and after solvent extraction show the CH_2 stretches of CTAB at 2850 and 2925 cm^{-1} and their depletion upon extraction. The smaller *d*-spacing in the extracted film suggests that siloxane condensation was incomplete and a contraction of the siliceous network occurred during extraction.

II. Properties of Azobenzene Derivatized with Bulky Dendrimers. The electronic absorption spectra of the azobenzene compounds in the visible and near UV contain peaks assigned to two electronic transitions: a strong $\pi-\pi^*$ transition and a weak $n-\pi^*$ transition. The phenyl substituents determine the exact position of these bands. For unsubstituted *trans*-azobenzenes the absorption maximum of the azo $\pi-\pi^*$ transition lies around 350 nm and the weak $n-\pi^*$ transition lies around 450 nm.[40] If the azobenzene compound is extended with extra phenyl groups (**AzoG1**, **AzoG2**, and **AzoG3**), the phenyl $\pi\pi^*$ absorption band becomes lower in energy (around 280 nm). *trans*-Azobenzene derivatives photoisomerize to cis compounds when they are excited at a wavelength where the trans to cis isomerization reaction is dominant over the cis to trans conversion. These conversion reactions are dependent on both the absorption of the two isomers at the excitation wavelength and the quantum yield of the different isomerization reactions at that wavelength. Excitation in the azo $\pi-\pi^*$ transition leads to an overall trans to cis isomerization, while excitation in the $n-\pi^*$ transition leads to an overall cis to trans conversion. The cis isomer can also thermally isomerize to the trans isomer: if a sample in the cis form is kept in the dark, it will eventually turn back into the trans form. The isomerization reaction is given by

$$\text{trans} \underset{\lambda_2,\Delta}{\overset{\lambda_1}{\rightleftharpoons}} \text{cis}$$

III. Properties of the Derivatized Azobenzene in Solution. *A. Rate of Thermal Back-Reaction.* The rates of the thermal back-reaction cis to trans and their yields for the compounds in Scheme 1 were studied in dichloromethane solution and are summarized in Table 1. The first-order rate constants can be calculated from the change in absorbance at a certain wavelength with time using the expression

$$k_\Delta t = \ln \frac{A_0 - A_\infty}{A_t - A_\infty} \tag{2}$$

where k_Δ is the thermal rate constant in s^{-1} and t is time in s. A_0, A_∞, and A_t are the observed absorbances of the solution at zero time, at the end of the reaction, and at time t, respectively. An example of such an experiment is shown in Figure 7. The inset gives the natural logarithmic plot of eq 2 with a linear fit, where the slope gives the thermal rate constant.

Most of the azo derivatives behave similarly, except for the rate constant of thermal **AzoOH** cis to trans isomerization. The larger rate constant can be ascribed to a deprotonation of the hydroxy group. If the hydroxy group is replaced by a methyl ether as in **$AzoOCH_3$**, then deprotonation is prevented and the rate constant is similar to those of the rest of the azo compounds.

A slightly higher rate constant for thermal isomerization, i.e., a faster isomerization reaction, is found for the small **AzoG0** molecule in comparison with that for the larger **AzoG3** molecule as expected due to the greater steric hindrance for the larger dendrimers. Nevertheless, the differences in rate constants for the molecules are small, even though their dimensions are very different. This similarity probably occurs because only the smaller methoxy group of the molecule, which is identical in all four cases, is actually moving during the isomerization reaction.

B. Isomerization Quantum Yields. The extinction spectra of the trans form for all the investigated compounds are determined from absorption spectroscopy. However, the extinction spectrum of the cis isomer cannot be directly calculated unless the exact concentration of the two forms during the photochemical experiment is known. Such data, the ratio between trans and cis forms, $r_{t/c}$, can be obtained by comparing the ^1H NMR spectra of a nonirradiated sample with that of an irradiated azo sample after a certain time t.[41,42] The cis extinction spectrum is then obtained using eq 3:

$$\epsilon_c = \left[\frac{A}{l} - \epsilon_t\left(c - \frac{c}{r_{t/c}+1}\right)\right]\left[\frac{r_{t/c}+1}{c}\right] \tag{3}$$

where A is the absorption of the irradiated sample and $r_{t/c}$ is the ratio between trans and cis isomers in the irradiated sample. Figure 8 shows the absorption spectra of both the trans and the cis forms of **AzoG1** in CH_2Cl_2 and their molar extinction coefficients. A correction for the thermal back-reaction must be applied if the cis form is not stable during the NMR measurement. The spectrum of the cis form and that of the photostationary state after irradiation at 344 nm are almost identical. In the photostationary state about 95% of the molecules are in the cis form, and 5% of the molecules are in the trans form. For all the other azo compounds these values are similar.

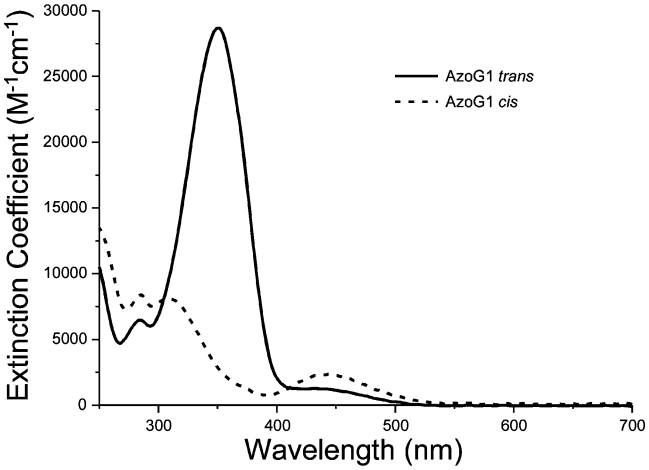

Figure 8. Extinction spectra of the trans and cis isomers of **AzoG1** calculated using eq 3.

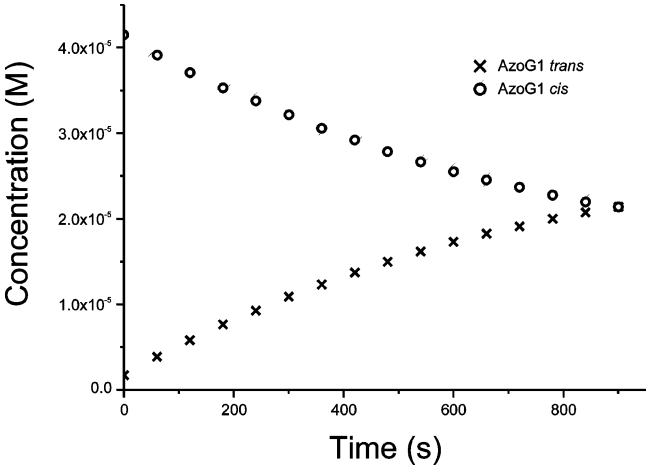

Figure 9. Concentration evolution of *trans*- and *cis*-**AzoG1**. A solution brought in the photostationary state by 344 nm light is subsequently irradiated at 450 nm for 900 s.

TABLE 2: Rate Constants for Thermal Isomerization of Azodendrimers G0−G3 Attached to Mesoporous MCM-41 in CH_2Cl_2 at Room Temperature

compound	k_Δ [s^{-1}]
AzoG0−MCM-41	1.02×10^{-5}
AzoG1−MCM-41	8.06×10^{-6}
AzoG2−MCM-41	6.92×10^{-6}
AzoG3−MCM-41	2.60×10^{-6}

Once the absorption spectra of both isomers are known, the yields of the nondominant isomerization reactions are calculated using the kinetic differential eq 4. All of the parameters can be obtained experimentally. This differential equation for the rate processes assumes monochromatic light, complete stirring, the Beer−Lambert law, and that the quantum yields in both directions are independent of I_0 and concentrations.[40]

$$\frac{dc_c}{dt} = I_0' \frac{1 - 10^{-A'}}{A'}(\epsilon_t' \varphi_{t\rightarrow c}' c_t - \epsilon_c' \varphi_{c\rightarrow t}' c_c) - k_\Delta c_c = -\frac{dc_t}{dt} \quad (4)$$

In this equation I_0', A', ϵ_t', ϵ_c', $\varphi_{t\rightarrow c}'$, and $\varphi_{c\rightarrow t}'$ are respectively the incident light intensity of the irradiation light, the absorption of the solution at the irradiation wavelength, the molar extinction coefficients of the trans and cis forms at the irradiation wavelength, and the quantum efficiencies of trans to *cis* photoisomerization and cis to trans photoisomerization at the irradiation wavelength.

In such an experiment the absorption spectra are taken as a function of time and the concentrations of the two isomers are calculated using the extinction coefficients of the trans and cis forms of the compound. The evolution of the concentration is shown in Figure 9 for **AzoG1**. These curves are analyzed by eq 4 to result in the isomerization yield data that are presented in Table 2. The results show unusual wavelength dependences for the quantum yields of isomerization, in violation of Kasha's rule, and have been previously observed for other azobenzenes.[43] Moreover, the isomerization yields decrease with the size of the molecules, as has already been mentioned, probably due to a steric effect.

C. Low Temperature Emission Spectra of Azodendrimer in Solution. Frozen glass emission spectra were taken with three purposes in mind: (1) to identify emission from the dendrimer as well as from the azo unit, (2) to control the concentration of azodendrimer in solution, and (3) to study the effect of the matrix. As can be seen from the emission spectra ($\lambda_{ex} = 351$ nm) of **AzoG3** in Figure 5A, at low concentration (0.05 mM) and low temperature (40 K), a structured emission centered around 450 nm is observed. As the concentration is increased (0.11 mM), emission centered around 600 nm grows in. Fluorescence emission at 600 nm in azobenzene-containing amphiphiles has been reported in an aqueous bilayer system.[44] It has also been reported that time-resolved fluorescence of an azobenzene-containing liquid crystal revealed an emission peak centered at 590 nm.[45] In both cases, the emission was assigned to the $S_1(n\pi^*)$ fluorescence of a J-like aggregate of azobenzene-containing amphiphiles. This emission is also seen in both surfactant filled and empty pores of the 2D hexagonal films and powders Figures 3A and 4A. This emission is most likely attributable to an aggregate of azodendrimers in the nanopores. Emission from the $S_2(\pi\pi^*)$ has also been observed at 420 nm.[45] In the case of **AzoG1**, dendrimer emission interferes with the ability to distinguish this S_2 emission (vide infra). At 0.55 mM and 40 K the molecule precipitates from solution and gives a red-shifted emission peak at 750 nm. At a concentration of 0.05 mM, as shown in Figure 5B, excitation at 457 nm produces an emission band with vibronic structure. This band is assigned to monomer emission from $S_1(n\pi^*)$. Increasing the concentration to 0.11 mM red shifts the emission and the vibronic structure is lost. At this concentration the $S_1(n\pi^*)$ excimer emission dominates. At 0.55 mM **AzoG3** has precipitated from solution and gives a broad peak centered around 720 nm.

To assist in the assignment of the emission bands, frozen glass samples of the Fréchet dendron (**G2**) were prepared. Figure 6 shows that structured emission from **G2** centered at 450 nm is similar to the structured emission from **AzoG3** when excited at 351 nm. This emission is band is thus assigned to the dendrimer and not the azobenzene unit. Also note that there is no concentration-dependent peak growing in at 600 nm, suggesting that the peak centered at 600 nm arises from the azo unit of the molecule and not the dendrimer. This assignment is confirmed by the large broad emission peak observed for **AzoOH** (no dendrimer attached).

IV. Absorption and Emission from Nanoconfined Azodendrimers. *A. Low Temperature Emission in Nanostructured Thin Films.* Azodendrimers tethered to the walls of nanopores exhibit luminescence properties similar to that from the molecules in solution. Using low temperature emission spectroscopy to study azodendrimer motion in 2D hexagonal thin films, reversible changes in the luminescence spectra are observed when exciting at 351 or 457 nm. Excitation at 351 nm ($\pi-\pi^*$) gives a concentration-dependent broad peak centered around 600 nm which is assigned to aggregate emission from $S_1(n\pi^*)$. Excitation at 457 nm produces an emission peak centered at 550 nm which is due to the $n-\pi^*$ monomer emission. Further evidence for this assignment comes from the frozen glass emission spectra of **AzoG3** (Figure 5B). At 0.05 mM the peak centered around 550 nm shows vibronic structure. If the emission spectrum excited at 457 nm were due to the excimer, no vibronic structure would be found. Similar emission spectra are observed for all generations of the azodendrimer molecules confined in nanopores.

B. Photoisomerization and Thermal Isomerization Reactions in Nanoconfined Environments. It is interesting to know if the photochemical properties change, and in particular if the photoisomerization reactions take place, when the azodendrimers are immobilized to a surface. The photochemical and thermal back-reactions of the azobenzene molecules confined in the nanostructured material and covalently bound to the inner walls of mesoporous MCM-41 particles are studied. The covalently

bound azo derivatives undergo efficient photoisomerization at about the same rates as they do in solution, and the thermal cis to trans isomerization still occurs. A suspension of the MCM-41 spheres can be studied in the same way as the solutions to determine the reaction constant of this thermal isomerization reaction using eq 2. Table 2 shows the rate constants of azo derivatives attached to the walls of MCM-41, suspended in CH_2Cl_2 at room temperature. It is interesting to notice that there is a significant effect on the rate due to the size of the dendrons. The bulky **AzoG3** compound has the smallest rate constant corresponding to the slowest reaction, while the smallest molecule **AzoG0** has the largest rate constant corresponding to the fastest reaction. It would be surprising if the entire **G3** dendron component of **AzoG3** undergoes the full range of possible motion. It is possible that some of the motion involves rearrangements of the part of the molecule between the dendron and the silicon atom at the pore wall. The observed rate constant for **AzoG3** is significantly smaller than that for the other derivatives. These results suggest that movement of the bulky dendron part of the azo molecules in the interior of the MCM-41 channels affects the isomerization rate. Such movement may lead to applications such as controlled blockage of a pore (nanovalve) or light-induced movement of unbound molecules (impeller).

Summary

A series of azobenzene derivatives has been synthesized. One end of the azo molecules is derivatized so that it can be attached to silica while the other end is derivatized with a certain generation of the Fréchet dendron (generation zero to generation three). The size and weight increase from **AzoG0** to **AzoG3**.

The photophysical properties of these molecules were examined in solution and frozen glass. The thermal cis to trans isomerization rate constant is similar for all generations of azo molecules ($k = 3.3 \times 10^{-6}$ s^{-1} for **AzoG0** to $k = 2.6 \times 10^{-6}$ s^{-1} for **AzoG3**) and can be understood as the small terminus of the molecule moving because it is the same for all azo molecules. The isomerization yields were calculated at the trans to cis (350 nm) and cis to trans (450 nm) isomerization wavelengths. With excitation at 344 nm, all generations of the azodendrimers have higher yields for the trans to cis isomerization than for the cis to trans. With excitation at 450 nm, the cis to trans isomerization has a higher yield than the trans to cis. Excitation at 344 nm predominantly gives the cis isomer, while excitation at 450 nm mainly gives the trans. These results depend not only on the isomerization yield but also on the molar absorptivity for each isomer at the excitation wavelength. The results show a wavelength dependence for the yield, in violation of Kasha's rule. Luminescence studies in frozen glass matrixes are used to identify emission from the azo unit as well as the dendrimer. Spectra of azobenzene without the dendrimer (e.g., **AzoOH**), with the dendrimer (e.g., **AzoG3**), and the Fréchet dendron without the azo unit (**G1**) are used to make assignments. Emission bands are similar for all generations of azodendrimers. With excitation at 351 nm, structured emission centered at 450 nm is observed and assigned to the dendrimer. A broad peak centered at 600 nm is assigned to the azo excimer. With excitation at 457 nm, nπ*emission from the azo unit is observed at 550 nm.

Properties of the molecules covalently attached to the pore wall of MCM-41 particles and 2D hexagonal silica films were also studied. The materials are characterized by XRD to confirm 2D hexagonal structure and estimate pore diameters. FTIR is used to monitor template removal. SEM is used to determine the diameter of the MCM-41 spheres. Large changes in the rate constants for the thermal cis to trans isomerizations of the azo derivatives are observed in the series of small **AzoG0** ($k = 1.02 \times 10^{-5}$ s^{-1}) to the large **AzoG3** molecule ($k = 2.6 \times 10^{-6}$ s^{-1}). This change implies that the dendrimer is moving and there is a clear dendritic effect. The low temperature emission spectra are similar to azo derivative emission in solution, suggesting that reversible isomerization (movement) occurs in the nanopores.

Acknowledgment. Financial support from the European Commission (IST-2001-35503) to L.D.C. and F.V., the National Science Foundation (DMR0346610 and CHE0507929) to J.I.Z., and MARCO-FENA (to J.I.Z.) is gratefully acknowledged. The XRD work was supported by the National Science Foundation under equipment Grant DMR-0315828. The authors thank UCLA undergraduates Sarah Koo and Kevin Leung and, at Bonn University, Friedhelm Luppertz for preparing some of the materials used in this study.

Supporting Information Available: Table showing time-dependent changes of the absorption spectra of **AzoG1**. This material is available free of charge via the Internet at http://pubs.acs.org.

References and Notes

(1) Liu, Z. F.; Hashimoto, K.; Fujishima, A. *Nature (London)* **1990**, *347*, 658−660.
(2) Sekkat, Z.; Dumont, M. *Appl. Phys. B: Laser Opt.* **1992**, *54*, 486−489.
(3) Liu, N.; Dunphy, D. R.; Atanassov, P.; Bunge, S. D.; Chen, Z. C.; López, G. P.; Boyle, T. J.; Brinker, C. J. *Nano Lett.* **2004**, *4*, 551−554.
(4) Liu, N.; Chen, Z.; Dunphy, D. R.; Jiang, Y.-B.; Assink, R. A.; Brinker, C. J. *Angew. Chem., Int. Ed.* **2003**, *42*, 1731−1734; *Angew. Chem.* 2**003**, *115*, 1773−1776.
(5) Hernandez, R.; Tseng, H.-R.; Wong, J.; Stoddart, J. F.; Zink, J. I. *J. Am. Chem. Soc.* **2004**, *126*, 3370−3371.
(6) Nguyen, T.; Tseng, H.-R.; Celestre, P.; Flood, A.; Liu, Y.; Stoddart, J. F.; Zink, J. I. *Proc. Natl. Acad. Sci. U.S.A.* **2005**, *102* (29), 10029−10034.
(7) Watson, S. J.; Gleeson, H. F.; d'Emanuele, A.; Serak, S.; Grozhik, V. *Mol. Cryst. Liq. Cryst. Sci. Technol., Sect. A: Mol. Cryst. Liq. Cryst.* **1999**, *331*, 2235−2242.
(8) Wirnsberger, G.; Scott, B. J.; Stucky, G. D. *Chem. Commun.* **2001**, *1*, 119−120.
(9) Ikeda, T.; Tsutsumi, O. *Science* **1995**, *268*, 1873−1875.
(10) Berg, R. H.; Hvilsted, S.; Ramanujam, P. S. *Nature (London)* **1996**, *383*, 505−508.
(11) Wang, J.; Stucky, G. D. *Adv. Funct. Mater.* **2004**, *14*, 409−415.
(12) Norikane, Y.; Tamaoki, N. *Org. Lett.* **2004**, *6*, 2595−2598.
(13) Ichimura, K.; Oh, S.-K.; Nakagawa, M. *Science* **2000**, *288*, 1624−1626.
(14) Calzaferri, G.; Huber, S.; Maas, H.; Minkowski C. *Angew. Chem., Int. Ed.* **2003**, *42*, 3732−3758; *Angew. Chem.* **2003**, *115*, 3860−3888.
(15) Chia, S.; Cao, J.; Stoddart, J. F.; Zink, J. I. *Angew. Chem., Int. Ed.* **2001**, *40*, 2447−2451.
(16) Miller, J. M.; Dunn, B.; Valentine, J. S.; Zink, J. I. *J. Non-Cryst. Solids* **1996**, *202*, 279−289.
(17) Dave, B. C.; Miller, J. M.; Dunn, B.; Valentine, J. S.; Zink, J. I. *J. Sol-Gel Sci. Technol.* **1997**, *8*, 629−634.
(18) Dunn, B.; Miller, J. M.; Dave, B. C.; Valentine, J. S.; Zink, J. I. *Acta Mater.* **1998**, *46*, 737−741.
(19) Chia, S.; Jun, U.; Tamanoi, F.; Dunn, B. S.; Zink, J. I. *J. Am. Chem. Soc.* **2000**, *122*, 6488−6489.
(20) Hernandez, R.; Franville, A.-C.; Minoofar, P.; Dunn, B.; Zink, J. I. *J. Am. Chem. Soc.* **2001**, *123*, 1248−1249.
(21) Minoofar, P. N.; Hernandez, R.; Chia, S.; Dunn, B.; Zink, J. I. *J. Am. Chem. Soc.* **2002**, *124*, 14388−14396.
(22) Minoofar, P. N.; Dunn, B. S.; Zink, J. I. *J. Am. Chem. Soc.* **2005**, *127*, 2656−2665.
(23) Victor, J. G.; Torkelson, J. M. *Macromolecules* **1987**, *20*, 2241−2250.
(24) Archut, A.; Vögtle, F.; De Cola, L.; Azzellini, G. C.; Balzani, V.; Ramanucham, P. S.; Berg, R. H. *Chem. Eur. J.* **1998**, *4* (4), 699−706.

(25) Kim, I.; Rabolt, J. F.; Stroeve, P. *Colloids Surf., A* **2000**, *71*, 167−174.

(26) Diameter and volume calculations were done using Chem 3D Ultra 8.0.

(27) Hawker, G. J.; Fréchet, J. M. J. *J. Am. Chem. Soc.* **1990**, *112*, 7638−7647.

(28) Fréchet, J. M. J.; Tomalia, D. A. *Dendrimers and other Dendritic Polymers*; Wiley-VCH: Weinheim, 2001.

(29) Schwyzer, R.; Sieber, P.; Zatsko, K. *Helv. Chim. Acta* **1958**, *60*, 491−498.

(30) Junge, D. M.; McGrath, D. V. *J. Am. Chem. Soc.* **1999**, *121*, 4912−4913. Junge, D. M.; McGrath, D. V. J. *Chem. Soc., Chem. Commun.* **1997**, 857−858.

(31) Haller, I. *J. Am. Chem. Soc.* **1978**, *100* (26), 8050−8055.

(32) Grün, M.; Lauer, I.; Unger, K. K. *Adv. Mater.* **1997**, *9* (3), 254−256.

(33) Van Tendeloo, G.; Lebedev, O. I.; Collart, O.; Cool, P.; Vansant, E. F. *J. Phys.: Condens. Matter* **2003**, *15*, S3037−S3046.

(34) Heller, H. G.; Langan, J. R. *J. Chem. Soc., Perkin Trans. 2: Phys. Org. Chem.* **1981**, *2*, 341−343.

(35) Willett, K. L.; Hites, R. A. *J. Chem. Educ.* **2000**, *77*, 900−902.

(36) Kresge, C. T.; Leonowicz, M. E.; Roth, W. J.; Vartuli, J. C.; Beck, J. S. *Nature* **1992**, *359*, 710.

(37) Lu, Y.; Garguli, R.; Drewian, C. A.; Anderson, M. T.; Brinker, C. J.; Gong, W.; Guo, Y.; Soyez, H.; Dunn, B.; Huang, M. H.; Zink, J. I. *Nature (London)* **1997**, *389*, 364−368.

(38) Huang,, M. H.; Dunn, B. S.; Soyez, H.; Zink, J. I. *Langmuir* **1998**, *14*, 7331−7333.

(39) Huang, M. H.; Dunn, B. S.; Zink, J. I. *J. Am. Chem. Soc.* **2000**, *122*, 3739−3745.

(40) Zimmerman, G.; Chow, L.-Y.; Paik, U.-J. *J. Am. Chem. Soc.* **1958**, *80*, 3528−3531.

(41) Tait, K. M.; Parkinson, J. A.; Bates, S. P.; Ebenezer, W. J.; Jones, A. C. *J. Photochem. Photobiol., A: Chem.* **2003**, *154*, 179−188.

(42) Tait, K. M.; Parkinson, J. A.; Jones, A. C.; Ebenezer, W. J.; Bates, S. P. *Chem. Phys. Lett.* **2003**, *374*, 372−380.

(43) Rau H. In *Studies in Organic Chemistry, Photochromism, Molecules and Systems*; Dürr, H., Bouas-Laurent, H., Eds.; Elsevier: Amsterdam, 1990; pp 165−191.

(44) Shimomura, M.; Kunitake, T. *J. Am. Chem. Soc.* **1987**, *109*, 5175−5183.

(45) Azuma, J.; Shishido, A.; Ikeda, T.; Tamai, N. *Mol. Cryst. Liq. Cryst.* **1998**, *314*, 83.